Natural Resources Canada
Ressources naturelles Canada

New insights on the geological and structural settings of the Musselwhite banded iron-formation–hosted gold deposit, North Caribou greenstone belt, Superior Province, Ontario

W. Oswald, S. Castonguay, B. Dubé, M. Malo, P. Mercier-Langevin, and J. Biczok

Geological Survey of Canada
Current Research 2015-3

2015

Canada

Geological Survey of Canada
Current Research 2015-3

New insights on the geological and structural settings of the Musselwhite banded iron-formation–hosted gold deposit, North Caribou greenstone belt, Superior Province, Ontario

W. Oswald, S. Castonguay, B. Dubé, M. Malo, P. Mercier-Langevin, and J. Biczok

2015

ISSN 1701-4387
Catalogue No. M44-2015/3E-PDF
ISBN 978-1-100-25348-0
doi:10.4095/295570

A copy of this publication is also available for reference in depository libraries across Canada through access to the Depository Services Program's Web site at http://dsp-psd.pwgsc.gc.ca

This publication is available for free download through GEOSCAN http://geoscan.ess.nrcan.gc.ca

Recommended citation

Oswald, W., Castonguay, S., Dubé, B., Malo, M., Mercier-Langevin, P., and Biczok, J., 2015. New insights on the geological and structural settings of the Musselwhite banded iron-formation–hosted gold deposit, North Caribou greenstone belt, Superior Province, Ontario; Geological Survey of Canada, Current Research 2015-3, 19 p. doi:10.4095/295570

Critical review
N. Pinet

Authors
W. Oswald (William.Oswald@ete.inrs.ca)
M. Malo (michel.malo@ete.inrs.ca)
Institut National de la Recherche Scientifique
Centre Eau-Terre-Environnement
490, rue de la couronne
Québec, Quebec
G1K 9A9

S. Castonguay
(Sebastien.Castonguay@RNCan-NRCan.gc.ca)
B. Dubé
(Benoit.Dube@RNCan-NRCan.gc.ca)
P. Mercier-Langevin
(Patrick.Mercier-Langevin@RNCan-NRCan.gc.ca)
Geological Survey of Canada
490, rue de la couronne
Québec, Quebec
G1K 9A9

J. Biczok(john.biczok@goldcorp.com)
Goldcorp Canada Ltd.
Musselwhite mine
P.O. Box 7500
Thunder Bay, Ontario
P7B 6S8

Correction date:

New insights on the geological and structural settings of the Musselwhite banded iron-formation–hosted gold deposit, North Caribou greenstone belt, Superior Province, Ontario

W. Oswald, S. Castonguay, B. Dubé, M. Malo,
P. Mercier-Langevin, and J. Biczok

Oswald, W., Castonguay, S., Dubé, B., Malo, M., Mercier-Langevin, P., and Biczok, J., 2015. New insights on the geological and structural settings of the Musselwhite banded iron-formation–hosted gold deposit, North Caribou greenstone belt, Superior Province, Ontario; Geological Survey of Canada, Current Research 2015-3, 19 p. doi:10.4095/295570

Abstract: The Musselwhite mine is a world-class gold deposit hosted in polydeformed amphibolite-facies banded iron-formation of the Mesoarchean North Caribou greenstone belt, northwestern Superior Province. The deposit is located about 2 km west of the tectonic boundary with the gneissic Island Lake domain. Detailed underground and surface mapping, core logging, and structural analyses have been undertaken to better characterize the various controls on gold mineralization.

The west antiform trench 1 and esker docks exposures show the dominant northwest-trending structural pattern related to the main (D_2) deformation phase. Multiple metre-scale type 3 F_1-F_2 and F_2-F_3 fold interference patterns are documented in the banded iron-formation. Coupled with regional-scale geological and U-Pb geochronological data, structural observations by the authors suggest that the mine area is located along the overturned limb of a kilometric-scale F_1 syncline that influenced the regional distribution and geometry of the prospective banded iron-formation units, preceding the main D_2 deformation.

Underground mapping of the 1045 main ramp and 770 level 11780N crosscut sections indicates that the ore, in the northern iron-formation, mainly occurs as stratabound pyrrhotite-rich replacements and associated quartz-flooding of the garnet-rich silicate banded iron-formation facies, and locally as discordant syndeformation quartz±pyrrhotite veins. The ore zones are associated with D_2-related high-strain zones, and are concentrated in hinges and along strongly attenuated limbs of F_2 folds. The composition of the garnet-rich silicate facies and layered mechanical anisotropy induced by competent banded iron-formation horizons embedded in less competent mafic and ultramafic volcanic rocks strongly influenced the deformation style and played an important role in controlling flow of gold-bearing fluids and formation and distribution of the ore.

Résumé : La mine Musselwhite est un gisement aurifère de classe mondiale encaissé dans une formation de fer rubanée polydéformée du faciès des amphibolites. Le gisement est situé au sein de la ceinture de roches vertes mésoarchéenne de North Caribou, dans le nord-ouest de la Province du lac Supérieur, à environ 2 km à l'ouest de la limite tectonique séparant la ceinture du domaine gneissique d'Island Lake. Afin de mieux caractériser les divers contrôles s'exerçant sur la minéralisation aurifère, nous avons entrepris des travaux détaillés de cartographie sous terre et en surface, la description de carottes de forage et des analyses structurales.

Dans l'antiforme Ouest, les zones d'affleurements de la tranchée 1 et des quais de l'esker révèlent une configuration structurale de direction nord-ouest dominante, liée à la principale phase de déformation (D_2). Plusieurs figures d'interférence de plis P_1-P_2 et P_2-P_3 de type 3, d'échelle métrique, ont été signalées dans la formation de fer rubanée. Conjuguées aux données géologiques à l'échelle régionale et aux données géochronologiques U-Pb, nos observations structurales donnent à penser que le secteur de la mine est situé le long du flanc inverse d'un synclinal P_1 d'échelle kilométrique, qui a influé sur la répartition régionale et la géométrie des unités prometteuses de la formation de fer rubanée, avant la déformation D_2 principale.

La cartographie sous terre des coupes transversales de la rampe principale au niveau 1045 et du travers-banc 11780N au niveau 770 indique que, dans la formation de fer Nord, le minerai se présente principalement sous la forme de zones de remplacement stratoïdes riches en pyrrhotite et de zones d'envahissement en quartz associées des faciès silicatés riches en grenat de la formation de fer rubanée, ainsi que, par endroits, sous la forme de filons de quartz±pyrrhotite discordants contemporains de la déformation. Les zones minéralisées sont associées à des zones de forte déformation apparentées à D_2 et se concentrent dans les charnières et le long des flancs considérablement amincis des plis P_2. La composition des faciès silicatés riches en grenat et l'anisotropie mécanique stratifiée, induite par l'existence d'horizons de formation de fer rubanée compétents encaissés dans des roches volcaniques mafiques et ultramafiques moins compétentes, ont exercé une forte influence sur le style de la déformation et joué un rôle important dans le contrôle de l'écoulement des fluides aurifères ainsi que dans la formation et la répartition du minerai.

INTRODUCTION

Banded iron-formation–hosted gold deposits are not as common as quartz-carbonate veins hosted in mafic volcanic rocks and intrusions, yet they have the potential to form world-class deposits (e.g. Homestake deposit, South Dakota, 40 million ounces Au (1244 t)). There are two end-member types of banded iron-formation-associated gold deposits (Dubé et al., 2011): those almost entirely banded iron-formation–hosted that commonly form large 'isolated' deposits (e.g. Musselwhite and Meadowbank mines), and those partially hosted in banded iron-formation, which are commonly part of a district associated with major fault zones (e.g. Meliadine (Nunavut) and Geraldton (Ontario) mining districts). The authors' research activity, part of the Targeted Geoscience Initiative 4 Lode Gold project of Natural Resources Canada, aims to study the geology of the Musselwhite banded iron-formation–hosted gold deposit, in particular, the controls on the formation and distribution of the mineralization and the geochemical footprint of the hydrothermal system (Dubé et al., 2011). The Musselwhite mine is one of the few banded iron-formation–hosted Archean gold deposits currently in production in Canada, and as such, it provides surface and underground exposure as well as abundant drill core and other geological data sets. It thus represents a highly suitable site to study banded iron-formation–hosted gold mineralization and improve understanding of this style of greenstone-hosted orogenic gold deposits (Robert et al., 2005; Dubé and Gosselin, 2007) in order to define key exploration vectors for similar mineralization in Canada.

The Goldcorp Canada Ltd.'s Musselwhite mine is located 475 km north of Thunder Bay and occurs in the North Caribou greenstone belt, part of the North Caribou Terrane of the western Superior Province (Thurston et al., 1991; Fig. 1). The Musselwhite mine started operation in 1997 and went over the threshold of 4 million ounces (124.4 t) of gold produced on August 1, 2014 (www.goldcorp.com [accessed November 17, 2014]). As of December 31, 2013, total proven and probable reserves for the Musselwhite mine are 1.85 million ounces (57.5 t) of gold (www.goldcorp.com); thus, at a yearly production rate of approximately 240 000 ounces (7.46 t), the expected mine life extends past 2021.

The authors' research thus far has mainly consisted in detailed surface and underground geological mapping and structural analyses. Systematic logging and sampling of drill cores has also been completed on a composite set of sections to provide petrographic and geochemical data across the

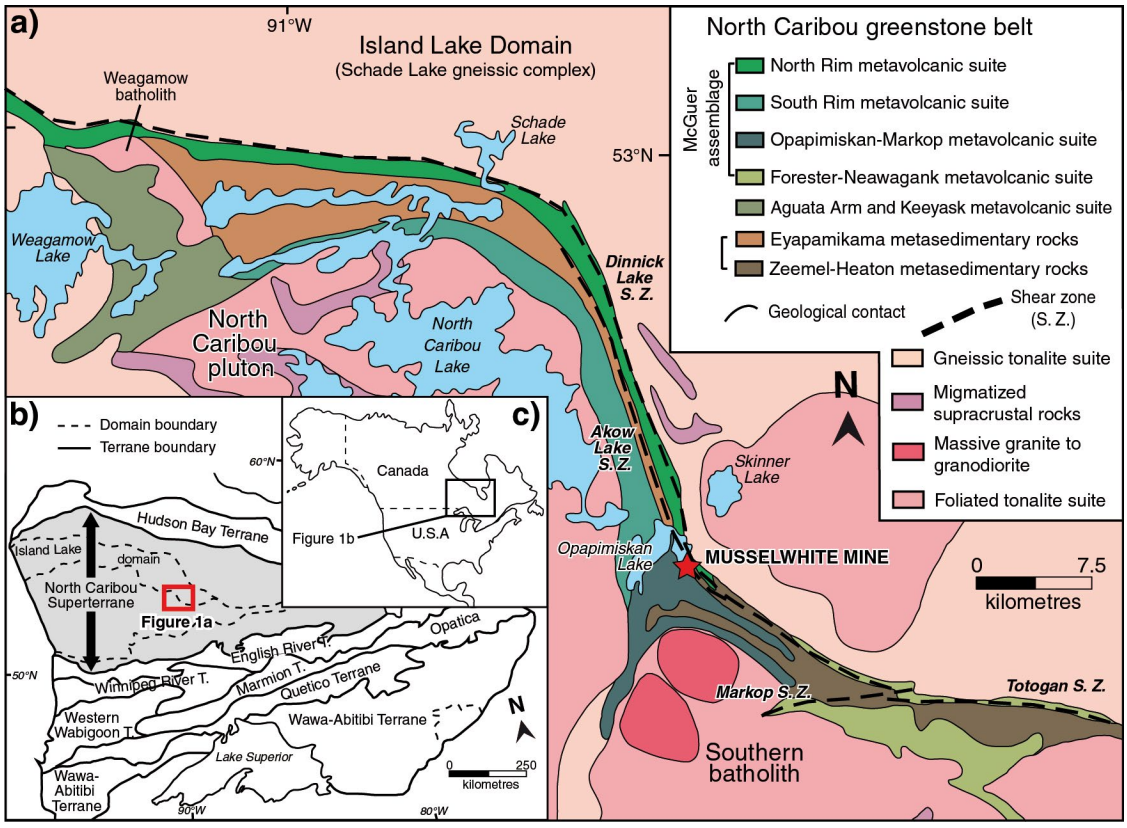

Figure 1. a) Simplified tectonostratigraphic map of the North Caribou Lake area *modified from* McNicoll et al. (2013), with insets showing **b)** tectonic setting within the western Superior Province and **c)** its geographic location in North America.

deposit. Although the present report focuses on the description of the geological and structural data and on the various controls on mineralization in the deposit area, preliminary observations regarding the alteration of host rocks and its footprint are also presented. The overarching study also includes activities such as targeted geochronology across most of the Opapimiskan Lake area (McNicoll et al., 2013; Oswald et al., 2014), which provide better constraints on the age of the host rocks, metamorphism, and major structural events.

GEOLOGICAL SETTING

The North Caribou greenstone belt, located in the central part of the North Caribou Terrane (Fig. 1), comprises rock units ranging in age from 3053 Ma to 2734 Ma (Davis and Stott, 2001; Biczok et al., 2012; McNicoll et al., 2013). The belt varies in width from 3 km to 7 km, over a length of about 60 km, and has a broad Z-shape comprising two roughly east-trending segments linked by a north-northwest-trending central part. It is constituted by ultramafic to felsic volcanic rocks and clastic or chemical sedimentary rocks in tectonic or intrusive contacts with the Island Lake gneissic complex (Island Lake domain) to the north and east, and with the Southern batholith and North Caribou pluton, to the south and west. Tectonic contacts with the Island Lake gneissic complex are marked by complex, probably long-lived, steeply dipping shear zones, with dominant late dextral kinematic events (Kalbfleisch, 2013).

Regional-scale mapping programs and studies (Breaks et al., 1985, 1991, 2001; Piroshco et al., 1989; Breaks and Bartlett, 1991; Thurston et al., 1991) have defined various lithostratigraphic assemblages in the North Caribou greenstone belt; from northwest to southeast (Fig. 1): the Agutua Arm metavolcanic suite, comprising mostly mafic metavolcanic rocks with minor felsic units (2981.0 ± 0.8 Ma; de Kemp (1987)); the metasedimentary and metavolcanic rocks of the Keeyask metavolcanic suite (2980.1 ± 3.0 to 2978.0 ± 3.0 Ma; de Kemp, 1987); the metasedimentary rocks of the Eyapamikama suite, which have maximum ages of 2962.6 ± 1.3 Ma to 2958.7 ± 1.8 Ma (de Kemp, 1987; Davis and Stott, 2001); the North Rim metavolcanic suite with maximum age of 2870 ± 2 Ma (Davis and Stott, 2001); the South Rim metavolcanic suite dated at 2981.9 ± 0.8 Ma (Davis and Stott, 2001); the Opapimiskan-Markop metavolcanic suite, dated at 2982.4 ± 0.8 Ma and 2972.4 ± 1.6 Ma (Biczok et al., 2012); the undated Forester and Heaton metavolcanic suites; and the 2853 ± 1 Ma and older Zeemel-Heaton metasedimentary suite (Davis and Stott, 2001). Active exploration work by Goldcorp Canada Ltd., around Opapimiskan Lake suggests that the South Rim and Opapimiskan-Markop volcanic suites are correlative and that their distinction is not relevant. Research and geochronology focused on batholiths surrounding the greenstone belt (*see* a compilation *in* Biczok et al. (2012)) shows that the Schade Lake gneissic complex and the North Caribou batholith are of similar ages, ranging between 2870 Ma and 2835 Ma, whereas the Southern batholith is significantly younger at ca. 2729–2723 Ma (Van Lankvelt, 2013). An older intrusion, the 2990 Ma Weagamow batholith (de Kemp, 1987) occurs in the northwest part of the greenstone belt.

Three main phases of regional deformation documented in the North Caribou greenstone belt (Satterly, 1941; Piroshco and Shields, 1985; Breaks et al., 1985, 1991) have resulted in complex fold interference patterns. The earliest event, D_1, consists of tight to isoclinal folds, associated with a penetrative S_1 foliation, commonly subparallel to bedding or layering (Breaks et al., 2001). D_2 is the dominant regional phase of deformation and consists of open to isoclinal shallowly northwest-plunging folds, coupled to a steeply dipping axial-planar foliation (S_2), frequently obliterating D_1 fabrics. D_3 structures are heterogeneously developed and are observed as asymmetric, broad, open or chevron folds, locally accompanied by a steep southwest-trending S_3 crenulation cleavage. Breaks et al. (1985) documented dome-and-basin–type fold patterns (type 1 of Ramsay and Huber (1987)) in the Opapimiskan Lake area and interpret them as the product of F_1 and F_2 fold interference, F_3 folds only causing a slight distortion. Such patterns have also been recognized in the present study, along with type 3 interference patterns. Major, probably long-lived or reactivated fault or shear zones often mark lithostratigraphic boundaries in the greenstone belt and overprint contacts with surrounding batholiths (Breaks et al., 2001).

The regional metamorphic grade varies from middle to upper greenschist facies in the northern part of the belt near Eyapamikama Lake (Breaks and Bartlett, 1991), to middle amphibolite facies around Opapimiskan Lake and farther east (Breaks et al., 1985). According to Hall and Rigg (1986), peak regional metamorphism occurred during the later stages of the D_2 deformation event. In the Opapimiskan Lake area, the metamorphic assemblage found in the iron-formation consists of various proportions of biotite, garnet, grunerite, staurolite, and pyroxene, compatible with an upper greenschist- to amphibolite-facies metamorphism (Klein, 2005). Thermobarometric studies indicate that peak metamorphism reached conditions of between 400–600°C and 3–7 kbars (Hall and Rigg, 1986; Breaks et al., 2001; Otto, 2002) before a late overprint of retrograde chlorite at about 250°C that has been documented at the Musselwhite mine (Otto, 2002). A narrow (≤0.5 km) amphibolitic contact aureole associated with the North Caribou pluton locally affects the regional metamorphic assemblage (Breaks et al., 1985, 1991).

LOCAL GEOLOGY

The Musselwhite deposit is hosted by isoclinally folded banded iron-formation of the Opapimiskan-Markop metavolcanic suite (Fig. 2), which includes two sequences of banded iron-formation units (Hollings and Kerrich, 1999; Breaks et al., 2001; Fig. 3a). The ore is mainly located in

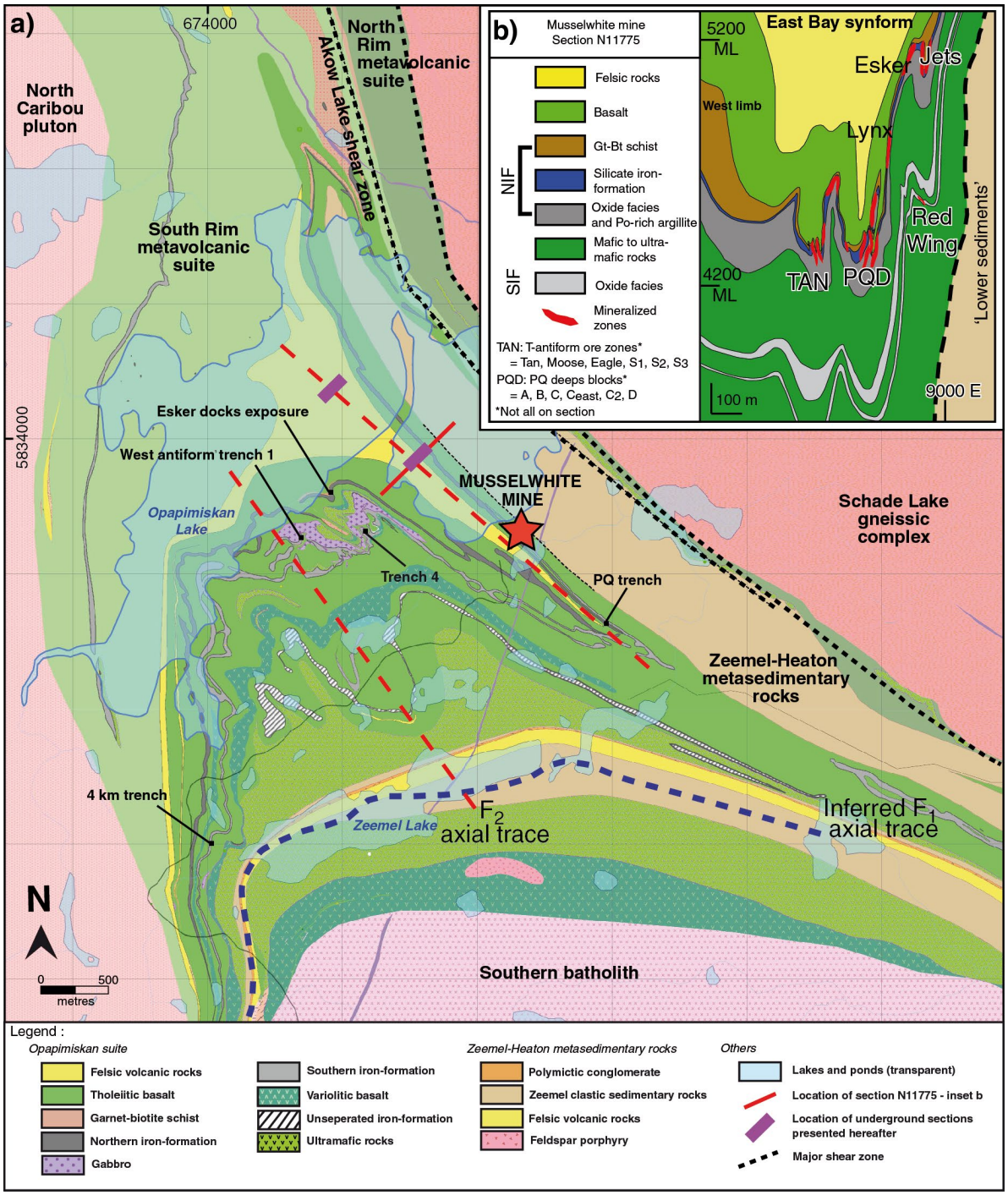

Figure 2. a) Geological map of the Opapimiskan Lake area (modified Goldcorp Canada Ltd., unpub. data compilation, 2014), with location of the studied surface exposures and underground levels (co-ordinates are in UTM NAD83 Zone 15). **b)** Simplified geological section of the mine at 11775N mine grid with location of the main ore zones. NIF = northern iron-formation, SIF = southern iron-formation, Gt = garnet, Bt = biotite, Po = pyrrhotite

the northern iron-formation with rather minor, but locally economical occurrences of gold mineralization in the southern iron-formation. The fundamental geological reasons for such mineralization partitioning between two neighbouring banded iron-formation units are part of the focus of the present study.

The northern iron-formation comprises several facies and metasedimentary units (Fig. 3b). The structurally lowest unit is a sulphide-rich meta-argillite (unit 4H) horizon overlain by chert-grunerite- (unit 4A) and chert-magnetite- (unit 4B) facies iron-formation. The 4B facies grades into a clastic facies containing garnet-amphibole beds interlayered with the chert-magnetite beds, which are overlain by a silicate-facies iron-formation (unit 4EA). Garnet-biotite schist (unit 4F), which contains a thin horizon of quartz-feldspar-biotite metasedimentary unit (unit 6), structurally overlies the iron-formation and a thin, garnet-bearing amphibolite (unit 4E) marks the transition into the volcanic rocks above. Units of 4F and 6 were both dated at younger than 2967 Ma (McNicoll et al., 2013). Felsic volcanic rocks (Avol), intercalated with minor ultramafic units, constitute the structural top of the Opapimiskan-Markop suite. They were dated by Biczok et al. (2012) at 2972.4 ± 1.6 Ma, which is much older than unit 6, indicating that the mine sequence manifestly is structurally inverted. A deformed felsic porphyry dyke dated at 2909.4 ± 0.7 Ma further refines the age constraint on the northern iron-formation, while also giving a maximum age for the main D_2 deformation event (McNicoll et al., 2013). Typical iron-formation units are usually Al_2O_3-poor (Klein, 2005). Preliminary geochemical data show that the various facies of the northern iron-formation contain 0.5–18 weight per cent Al_2O_3, 20–40 weight per cent total Fe_2O_3, and 45–67 weight percent SiO_2. The Al_2O_3 can be used to infer a detrital input, or contamination, of the iron-rich, chemical sedimentary rocks (Klein, 2005). Here, the temporal evolution of the northern iron-formation sequence illustrates a decreasing clastic input and an increase in the hydrothermal component, expressed by the total Fe_2O_3 and SiO_2 contents (Fig. 3b).

The southern iron-formation (Fig. 2a, 2b, 3a) consists of two major horizons of chert-magnetite- and chert-grunerite-facies iron-formation (G. Couture, unpub. report, 1995; S. Blower and J. Kiernan, unpub. technical report, 2003; Moran, 2008). Surface exposures of the southern iron-formation show that the thin (0.8 m to a few metres) chert-magnetite facies lies at the structural top of the sequence, whereas the

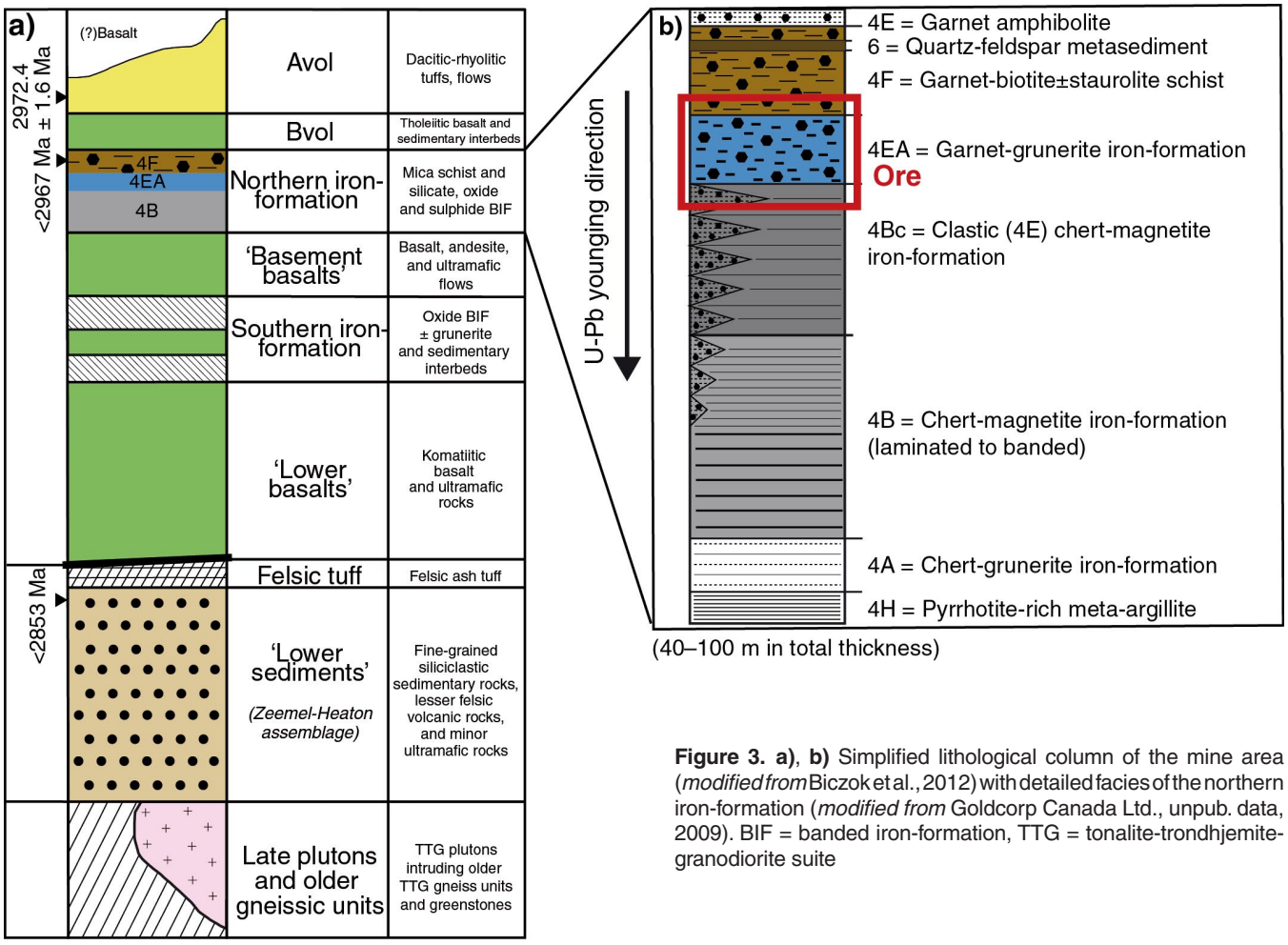

Figure 3. a), b) Simplified lithological column of the mine area (*modified from* Biczok et al., 2012) with detailed facies of the northern iron-formation (*modified from* Goldcorp Canada Ltd., unpub. data, 2009). BIF = banded iron-formation, TTG = tonalite-trondhjemite-granodiorite suite

chert-grunerite±magnetite facies can reach several tens of metres in thickness. The chert-grunerite±magnetite facies is notably chert-rich and interbedded with fine-grained, light- to medium-brown, amphibole-rich clastic beds. These beds locally weather green, suggesting a predominantly mafic source rock, which is consistent with the lithologies intercalated with the southern iron-formation horizons. Complex soft-sediment deformation structures are locally present. The age of the southern iron-formation is not known, but based on recent geochronological data (McNicoll et al., 2013), it is interpreted to be younger than the northern iron-formation.

DETAILED SURFACE MAPPING: CHARACTERIZING THE MAIN STRUCTURAL ELEMENTS

Detailed mapping and structural analysis of key surface trenches in the mine area and underground workings have been undertaken to better understand the geometry and structural controls of the deposit and its host rocks. Two exploration trenches (stripped outcrops) have been mapped in detail using a high-precision GPS (Promark 800, Ashtech). These sites were chosen in areas of lower D_2 strain, providing more favourable conditions to document D_1-related structures, their interference with the main D_2 deformation, and their possible significance ('ground preparation') on the distribution of the units hosting the bulk of the gold mineralization.

Esker docks exposure

The esker docks exposure (Fig. 4a) is a 50 m^2 stripped outcrop of the northern iron-formation on the south shore of Opapimiskan Lake, about 1.5 km west of the Musselwhite mine (Fig. 2a). Structurally, it is located on the northeastern part of the west antiform. The outcrop solely exposes the 4F unit, which comprises fine-grained biotite-rich layers with medium-grained garnet porphyroblasts, and about 1 cm thick chert layers in an approximate proportion of 75–25% respectively (Fig. 5a). Subhedral to euhedral almandine garnet porphyroblasts constitute 10–40% of individual layers and are unevenly distributed in the biotite-rich matrix. They tend to be more abundant in the vicinity of the chert bands. The weathering patina is beige, but green in some layers, which suggests mineralogical variations in the metamorphic paragenesis.

A S_1 foliation is locally preserved along the hinges of F_2 folds (Fig. 5b). In addition, refolded folds are present in the southern and southwestern corners of the outcrop (Fig. 5c, 5d) where F_1 folds are wrapped around the F_2 folds, in a

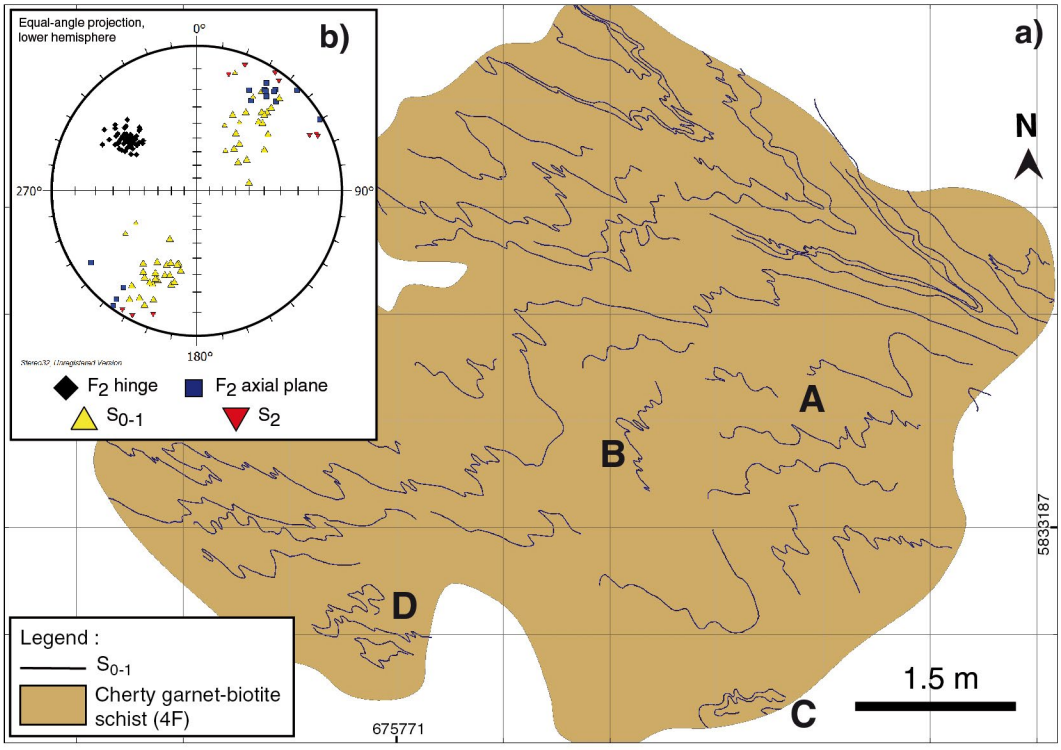

Figure 4. a) Map of the esker dock outcrop, outlining the S_{0-1} layering and main folding pattern. **b)** Stereographic projection (lower hemisphere) of structural measurements. Labels A to D refer to the location of photographed structural features shown in Figure 5.

manner similar to the type 3 interference pattern of Ramsay and Huber (1987). As mentioned by Breaks et al. (2001), such a pattern suggests that axial planes of the F_1 folds were originally shallowly dipping, and at high angle with the F_2 axial planes.

The dominant structural pattern is that of asymmetrical, open to tight, mesoscopic F_2 folds that have shallowly northwest-plunging axis and upright fold axial plane (Fig. 4b). The fold geometry and orientation are similar to those described by Breaks et al. (2001) in the Opapimiskan Lake area. Short limbs more frequently include parasitic folds. Z-, M-, and S-type folds are present throughout the exposure (Fig. 5a). Folds are associated with a well developed, upright, northwest-trending S_2 foliation (280° to 330°; Fig. 4b), especially in the biotite-rich layers. The outcrop structural pattern, constituted of a set of broad antiforms and adjacent tight synforms, is closely similar to the regional pattern in the Opapimiskan Lake area (Fig. 2a). No evidence of structures postdating D_2 was observed.

West antiform trench 1

The west antiform trench 1 is located 2 km west of the mine camp, in the hinge zone of the west antiform, an area of lower D_2 deformation intensity where older fabrics are better preserved than in the mine vicinity (Fig. 2a). The stripped outcrops expose chert-magnetite banded iron-formation interlayered with komatiitic basalt and gabbroic sills (Fig. 6a). Based on the regional aeromagnetic map, the exposed iron-formation is interpreted to be part of the southern iron-formation.

The outcrop illustrates the influence of competency differences between the iron-formation and the volcanic rocks on the structural style and strain response. Structural variations include F_2 fold tightness, the development of the S_2 foliation in the banded iron-formation, and most notably the preservation of the S_1 foliation. In the chert-magnetite banded iron-formation, which has a higher competency than that of the garnet-biotite facies at the esker docks outcrop,

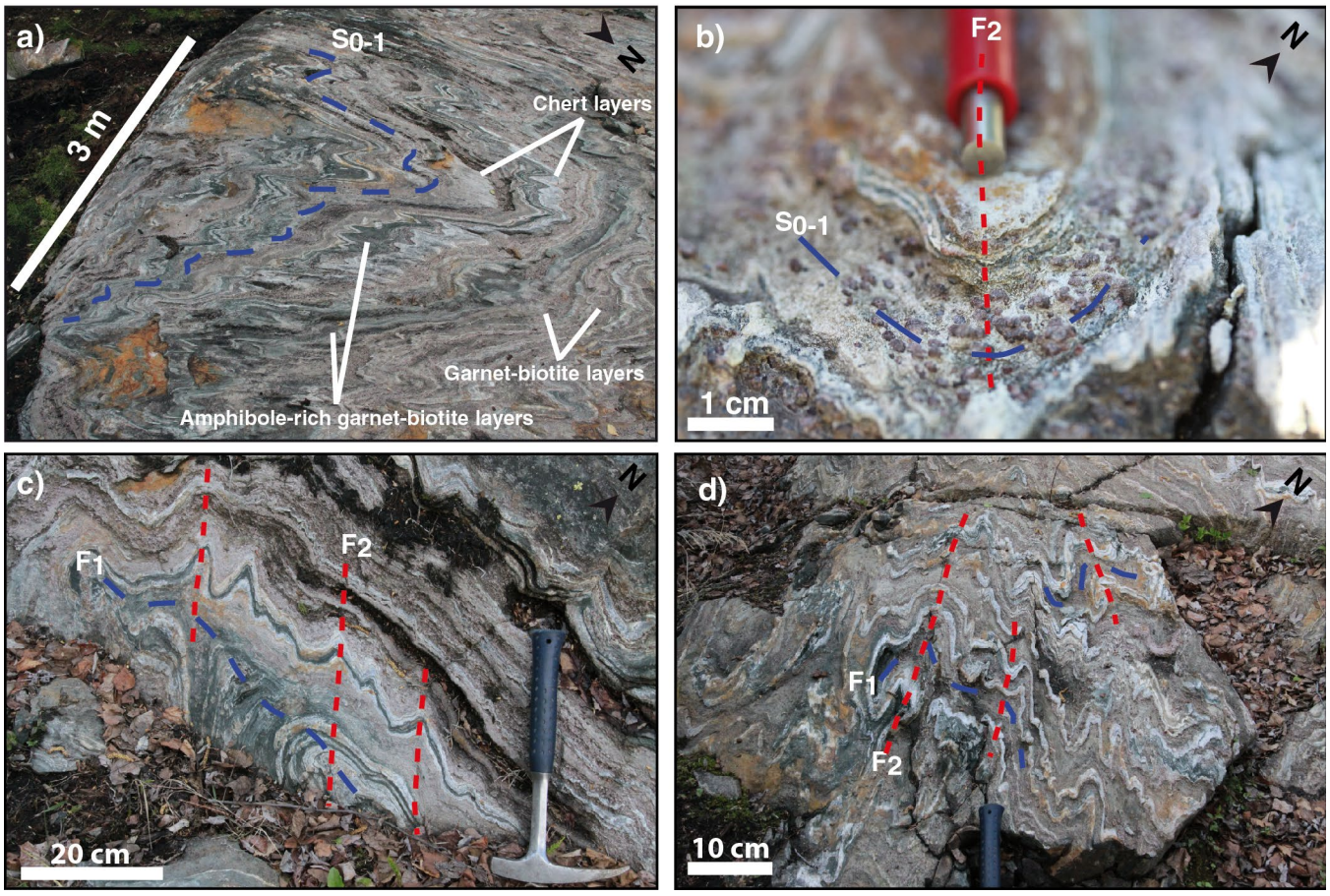

Figure 5. Photographs of the esker docks exposure (*see* Fig. 4 for locations). **a)** S_{0-1} layering in cherty garnet-biotite schist folded by a metre-scale F_2 fold (view looking southwest); 2014-199; **b)** close-up view of the S_1 foliation in a garnet-biotite band along a F_2 hinge; 2014-198; **c)** and **d)** F_1 folds affected by F_2 folds creating type 3 interference pattern in cherty garnet-biotite schist. Blue dashed lines are F_1 axial planes; Red dashed lines are F_2 axial planes. 2014-208, 2014-205, respectively. All photographs by W. Oswald.

the S_1 foliation is best distinguished in cherty bands along the hinge zone of F_2 folds. In the volcanic rocks, the S_1 foliation is ubiquitous and penetrative. Decametre-scale to mesoscopic F_1 isoclinal folds are also locally preserved. For example, a thin iron-formation layer in the volcanic rock that is involved in a F_1 fold (Fig. 6a) is refolded by an F_2 fold, producing a type 3 interference pattern (Fig. 7a). Similar small-scale fold-pattern examples are present in the iron-formation.

The dominant structural pattern is related to D_2 deformation. In the volcanic rocks, the S_1 foliation is folded by centimetre- to decimetre-scale, close, locally chevron-style, upright F_2 folds. The relationship between S_1 and F_2 folds suggests that S_1 was initially shallowly dipping (Fig. 7c). In the banded iron-formation, the S_1 foliation is folded by open to tight F_2 folds, locally isoclinal, with steeply dipping to upright axial planes. F_2 axes are generally plunging between 25° and 50° to the west-northwest (i.e. 270° to 320°; Fig. 6b), and some plunge 10–50° to the

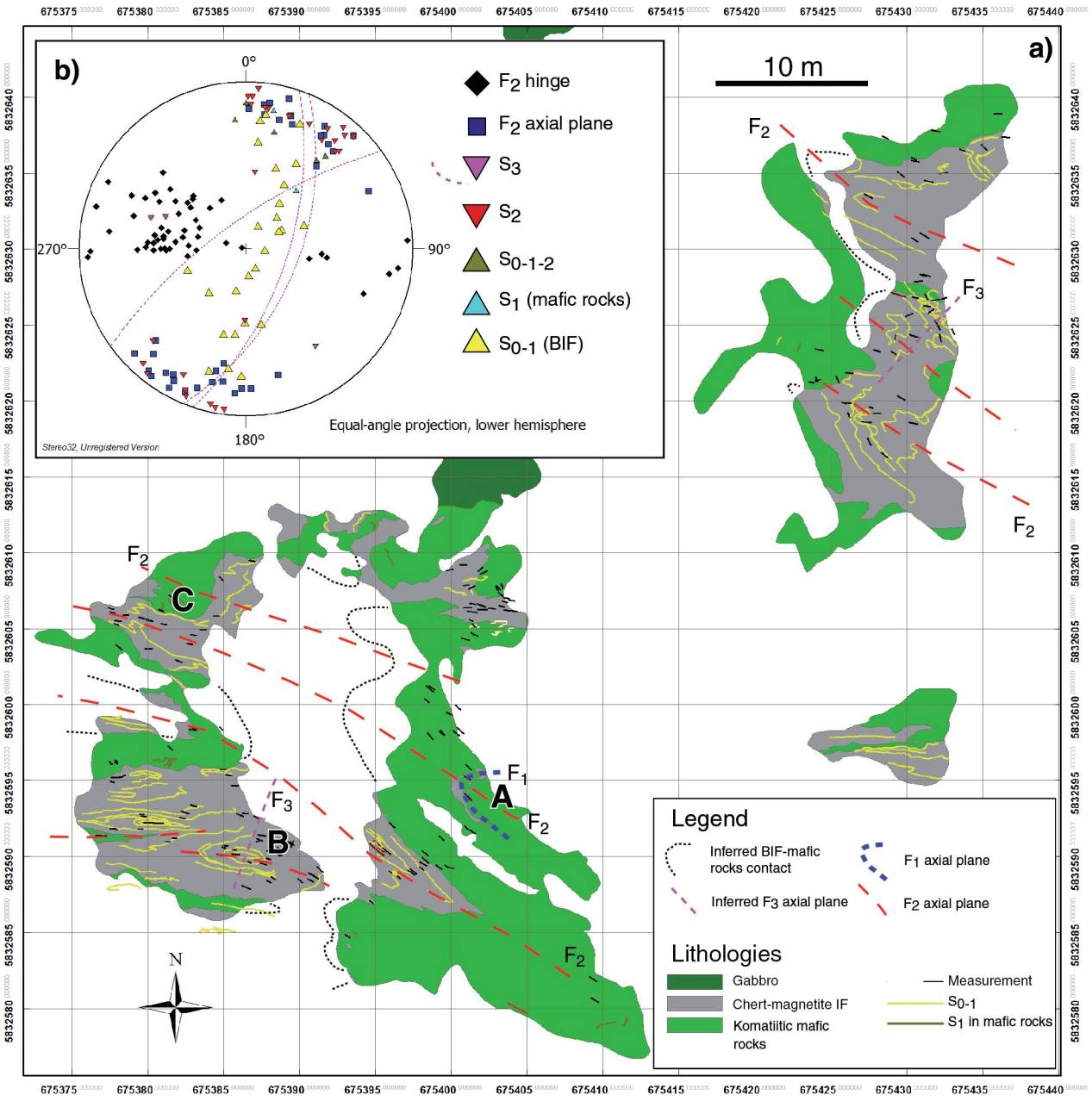

Figure 6. a) Geological map of the west antiform trench 1 exposure. **b)** Stereographic projection (lower hemisphere) of structural data. Labels A to C refer to the location of photographed structures in Figure 7. IF = iron-formation, BIF = banded iron-formation

east-southeast (Fig. 6b). Figure 7b shows an example of such doubly plunging F_2 folds. The significance of such measurements will be discussed below. Stereographic projections of the composite S_{0-1} orientation in the iron-formation tend to define a great circle with a pole plunging 20° toward 285° (Fig. 6b), compatible with orientation of measured F_2 folds. Parasitic F_2 folds are common, although in areas of higher strain intensity such as the southwestern part of the exposure, these frequently have sheared limbs. The S_2 fabric varies from a spaced cleavage in low-strain areas to a penetrative foliation in more deformed areas, such as in the iron-formation.

A moderately to steeply dipping, northeast-trending S_3 crenulation cleavage is locally present. It is best developed in magnetite-rich layers, which are less rigid than the adjacent chert beds. F_3 folds are scarce and inconspicuous, although some are interpreted based on the occurrence of doubly plunging F_2 folds (Fig. 7b). A broad, open F_3 antiform is also evidenced by southeast-plunging F_2 hinges on the northeastern portion of the exposure (Fig. 6a).

UNDERGROUND MAPPING: DOCUMENTING STRUCTURAL CONTROLS ON MINERALIZATION

Two underground sections were mapped in detail to document the mineralization and its stratigraphic and structural controls, as well as the different structural styles induced by the rheological contrasts between the iron-formation host rock and the surrounding volcanic sequences.

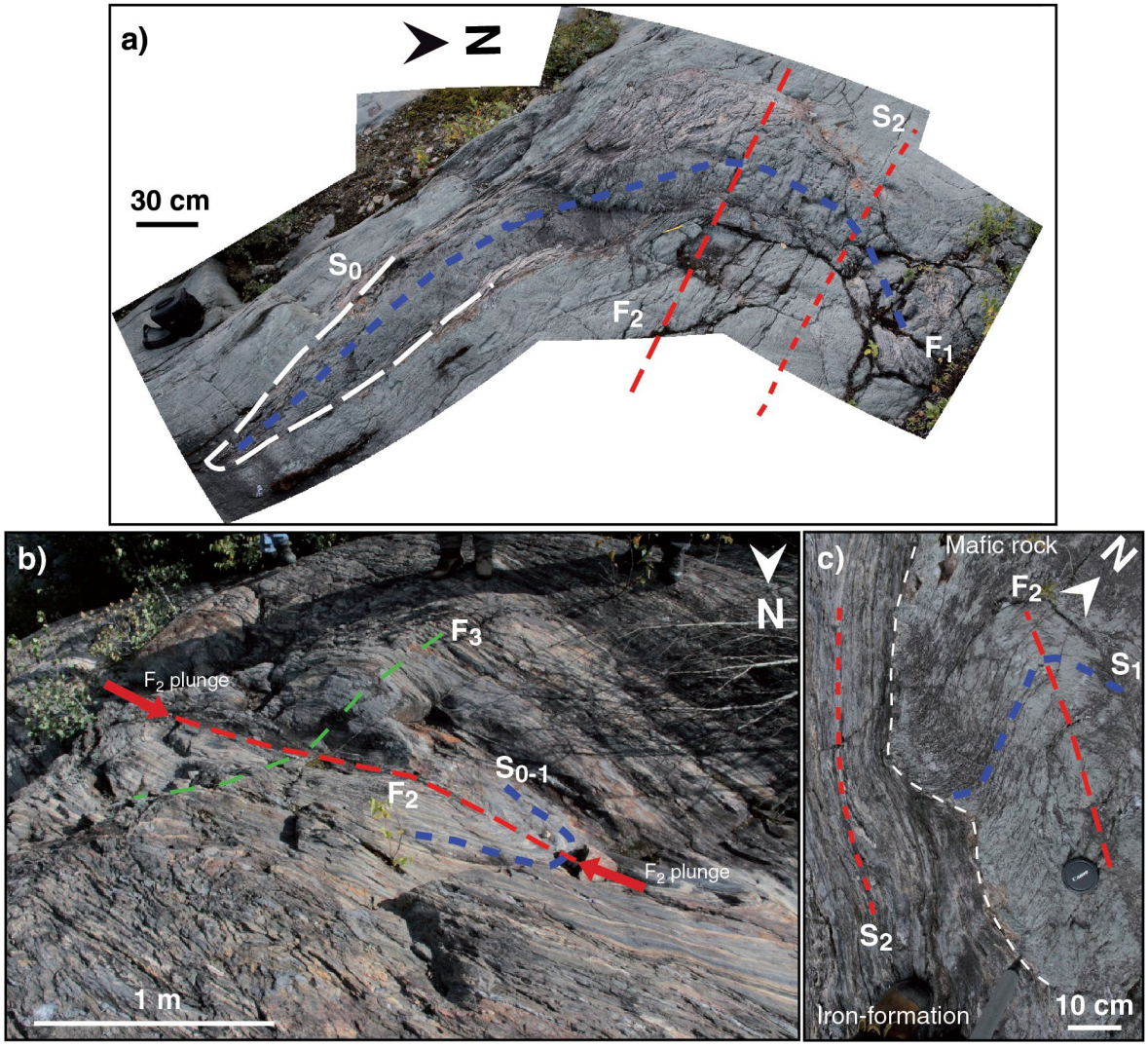

Figure 7. Photographs of representative structural features of the west antiform trench 1 exposure. **a)** Mesoscopic F_1 outlined by a layer of chert-magnetite iron-formation, refolded by a F_2 fold; 2014-200; **b)** northwest-trending doubly plunging F_2 fold in chert-magnetite iron-formation; 2014-201; **c)** plan view of the contact between chert-magnetite iron-formation (left side) and mafic volcanic rocks (right side); note the different structural styles and preserved S_1 in the volcanic rocks, induced by the competency contrast between units; 2014-204. All photographs by W. Oswald.

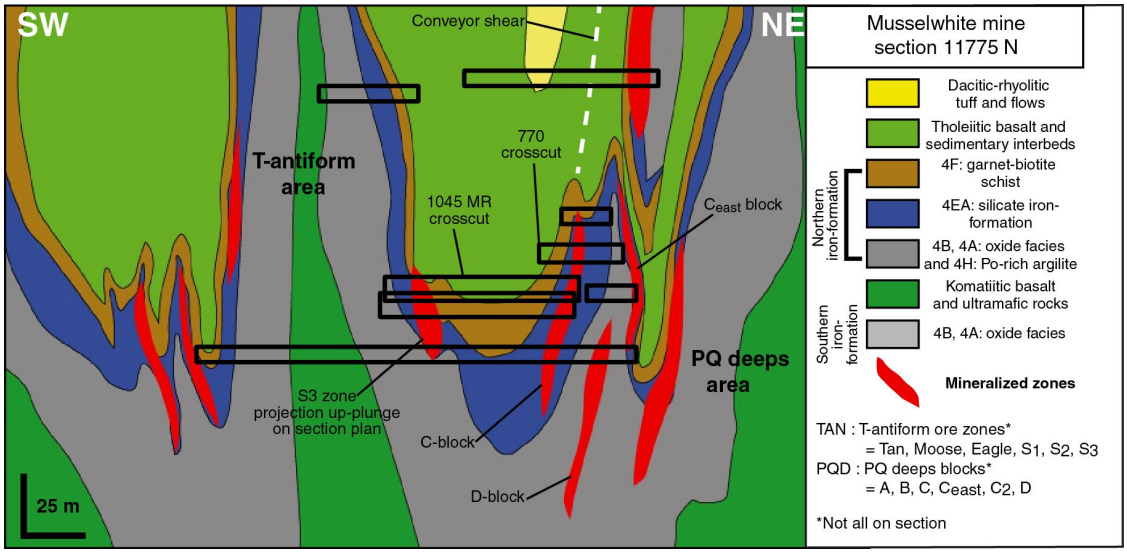

Figure 8. Simplified geology of the N11775 section in the PQ deeps and T-antiform areas, Musselwhite mine. Ore zones are shown in red and the locations of the mapped underground crosscuts are marked by black rectangles. The labelled crosscuts are those presented in this report. Po = pyrrhotite

1045 main ramp section

The 1045 main ramp section is located immediately to the east of the main ramp on mine grid section 12900, which approximately projects at surface to the middle of Opapimiskan Lake, between the esker peninsula and the north shore (Fig. 2a). The section is 82 m long and extends westward from the PQ deeps C-block ore zone, to the east limb of the T-antiform (Fig. 8). The western part of the section offers a good exposure of the northern iron-formation sequence and the transition from detrital-dominated facies (4F±4EA) to hydrothermal-dominated facies (4B±4Bc; Fig. 9). Along the section, a tholeiitic metabasalt structurally overlies the northern iron-formation. Competency contrasts are evident between the intensely folded iron-formation facies and the massive-looking volcanic rock. Based on the relationships between S_0, S_1, and S_2 mapped on surface exposures, the layering in the various iron-formation facies present underground is referred to as S_{0-1}, although strong transposition parallel to S_2 locally occurs. Otherwise, D_1 structural features have not been clearly distinguished.

F_2 folds occur at different scales along the section, which lies in the hinge area of a large synform involving the whole northern iron-formation sequence (Fig. 8, 9), and that constitutes the eastern part of the East Bay synform, west of the T-antiform. Along the moderately to steeply dipping western limb (from 0 to 35 m), S_{0-1} measurements are predominantly east dipping (300–320°/60–75°), whereas the eastern limb measurements (from 75 m) dip steeply to the west (130–140°/80–88°; *see* Fig. 11a). Based on all S_{0-1} measurements, the orientation of the fold hinge is calculated at 315°/20°. A metre- to decametre-scale series of antiform-synform parasitic folds is present from 30 m to 65 m (Fig. 9), involving the garnet-biotite schist and the mafic volcanic rocks (including its biotite altered facies). Between 35 m to 50 m, the south side of the gallery provides an outstanding exposure of the keel of a synform, outlined by the folded contact between the garnet-biotite schist and volcanic rocks (Fig. 9). Numerous decimetre-scale shallowly northwest-plunging asymmetric F_2 folds (axes at about 300–320°/20–30°; *see* Fig. 11a) are confined to the banded iron-formation facies. They are mostly S-shaped on the northeastern limb of the T-antiform. Fewer folds are present on the C-block side due to higher strain and reduced exposure of the iron-formation. Axial planes of F_2 parasitic folds frequently dip steeply to the west, and become vertical in higher strain zones.

There is little data on gold grades along the 1045 main ramp section. Quartz-pyrrhotite veins and quartz-flooding are around 18–25 m in the garnet-grunerite and garnet-biotite units (Fig. 9), and assays from nearby drill hole 12-TAN-096 give minor 1–3 ppm gold grades. Quartz-pyrrhotite veins and quartz flooding are also particularly abundant around 40 m, where the crosscut section lies 25 m above the S3 ore zone, along the lower eastern limb of the T-antiform (Fig. 8). At around 40 m, strong quartz flooding is accompanied by coarser garnet crystals in 4F unit. In contrast, the overlying and less competent mafic rocks comprise quartz-pyrrhotite±carbonate veins. In the vicinity of the C-block ore zone, at the far end of the section (~75 m), minor pyrrhotite mineralization is present in the 4F unit. Adjacent mafic volcanic rocks become increasingly strained eastward and display a strong biotite alteration and increasing quartz±carbonate

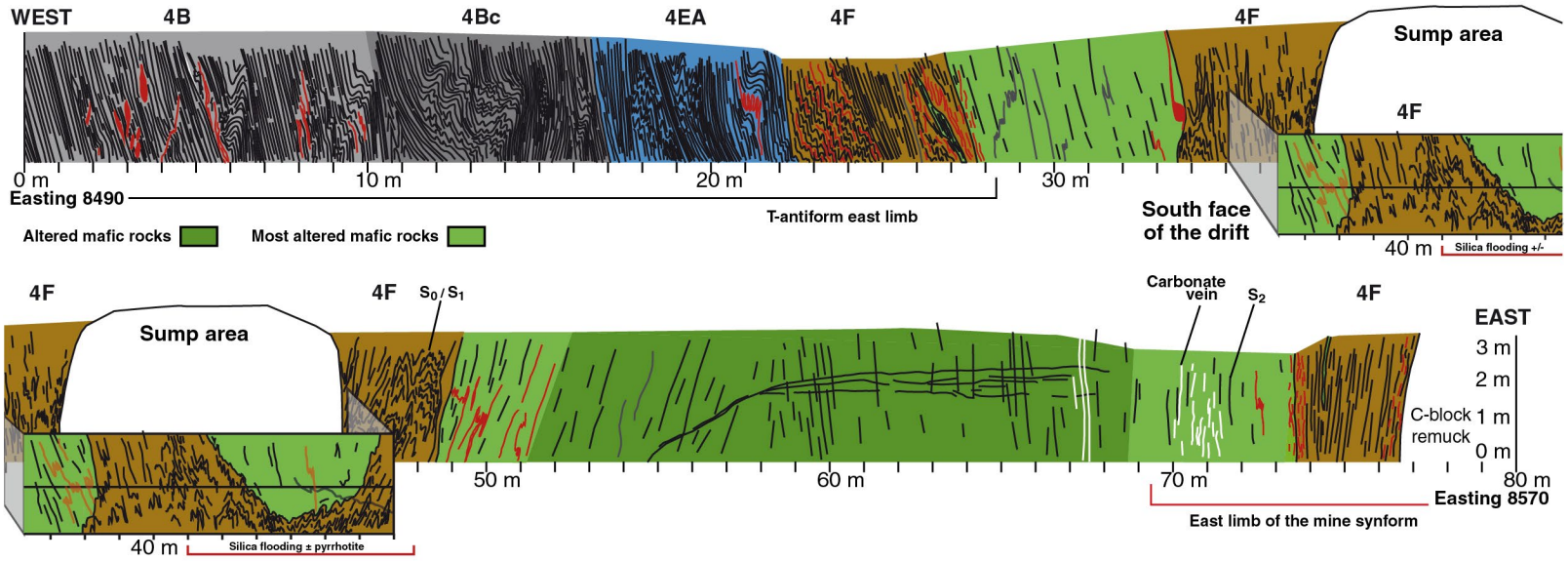

Figure 9. Geology of the northern wall of the 1045 level main ramp crosscut.

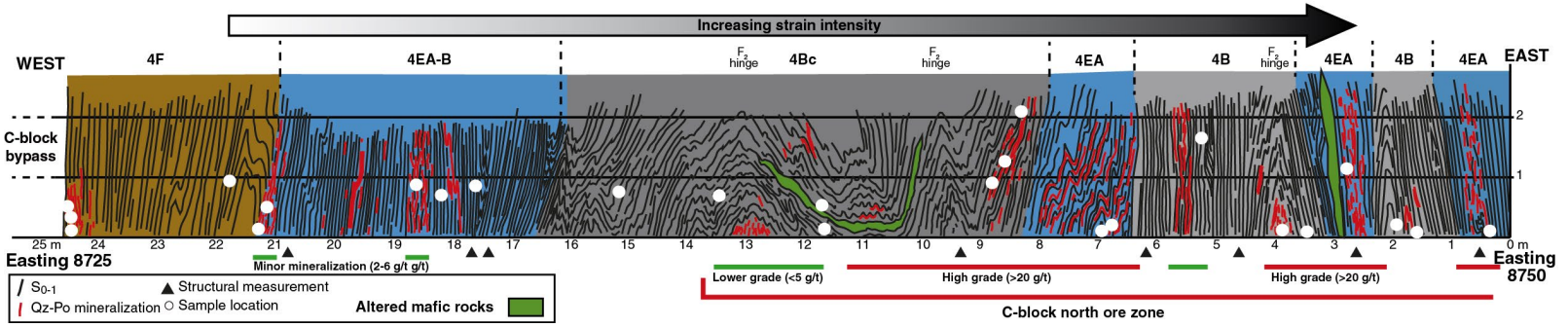

Figure 10. Geology of the northern wall of the 770 level 11780N crosscut. Qz = quartz, Po = pyrhotite

veining approaching the unit 4F contact. This calcite-rich high-strain zone is consistently intercepted in diamond-drill holes and termed the 'conveyor shear' (Fig. 8, 9). It lies along the east limb of the East Bay synform, roughly parallel to its axial plane. This high-strain zone is barren except where it affects gold-bearing iron-formation lenses (4E unit) intercalated in the mafic sequence. This relationship, and the relative timing of calcite-rich alteration with respect to biotite alteration, suggests that this structure focused fluid flow during a late- to post-mineralization CO_2-rich hydrothermal phase.

770 level 11780N crosscut

The 770 level 11780N crosscut exposes the C-block ore zone and is located between the C_{east}-block of the PQ deeps zone and the mafic volcanic rocks overlying the northern iron-formation sequence (Fig. 8). The crosscut is 25 m long and exposes several banded iron-formation facies (Fig. 10), including the chert-magnetite iron-formation (unit 4B), the chert-magnetite-garnet-amphibole (unit 4Bc), the garnet-grunerite (unit 4EA), the garnet-biotite schist (unit 4F), as well as some interlayered mafic rocks (unit 2T).

The structure of the section is dominated by penetrative D_2 fabrics with a strong eastward-increasing deformation gradient. In areas of lower D_2 strain, S_{0-1} is locally differentiated from the axial-planar S_2 fabric associated with close to upright shallowly northwest-plunging F_2 folds (Fig. 11b). Otherwise, the S_{0-1} layering in the 4B facies is dominantly transposed into the subvertical S_2, with only a few preserved tight to isoclinal rootless folds (e.g. Fig. 12a). Folds within clastic 4B and 4EA facies are dominantly open, especially from 10 m to 25 m (Fig. 10), where strain is less intense. The 4F unit only displays rare folds, except close to the contact with unit 4EA, where folding is ubiquitous. Contacts between the 4B and 4EA facies are marked by D_2 high-strain zones. Such structural style differences between units combined with minor gold grades associated with quartz-pyrrhotite mineralization suggest that lithological contacts acted as décollement surfaces that focused strain and facilitated hydrothermal fluid flow. For instance, the 4Bc-4EA contact at 16.5 m contains 4 ppm of gold according to the chip sampling and the 4EA-4F contact at 21.3 m contains 2.8 ppm (Fig. 10). The sharp increase in gold grade at 6.5 m between the 4B and 4EA facies (Fig. 10) also illustrates the influence of lithological facies on gold mineralization (*see also* Fig. 12a).

The eastern half of the section exposes part of the C-block, where most of the gold ore occurs in the 4EA facies. Quartz-pyrrhotite-carbonate mineralization is closely associated with subvertical high-strain zones and adjacent tight to open folds that likely acted as zones of lower pressure during deformation and mineralization (Fig. 12b). F_2 folding was accompanied by the emplacement of axial-planar to low-angle quartz veins, bedding-parallel veins, low-angle tension gashes fanning around folds hinges, and locally by discrete axial-planar brittle faults offsetting fold hinges (Fig. 12c). The 4Bc facies, which is rheologically similar to unit 4EA,

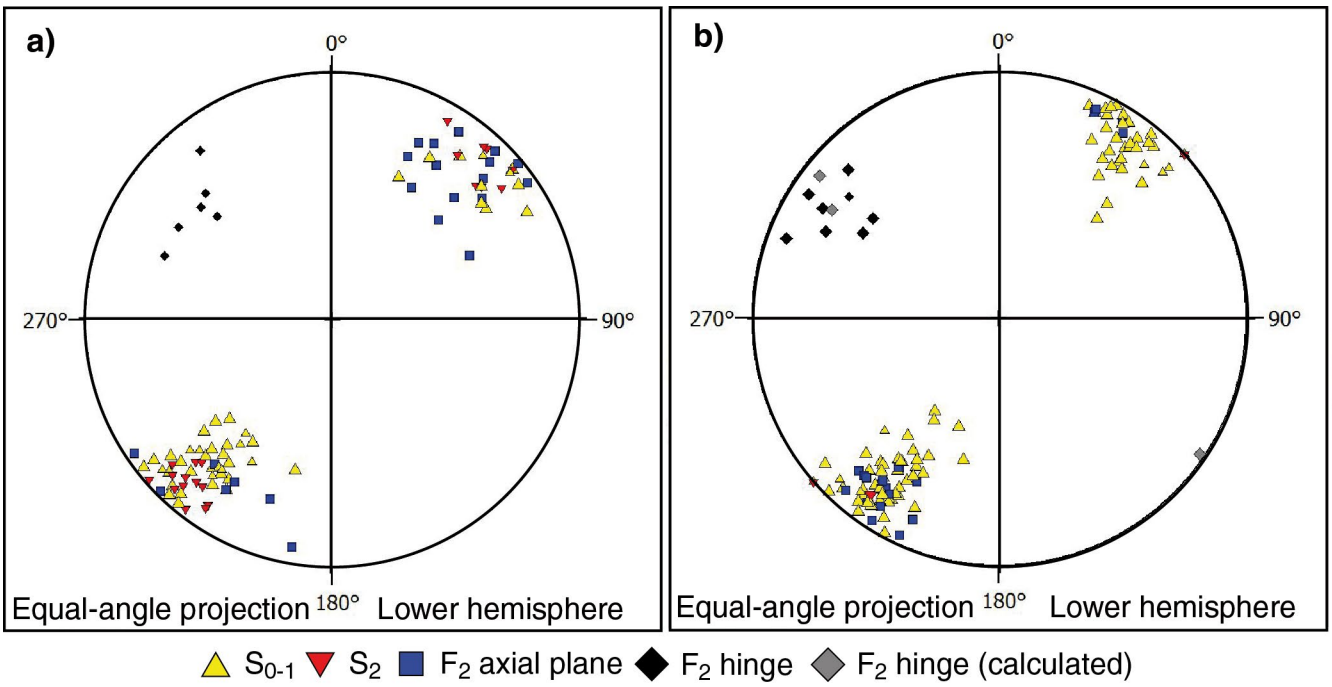

Figure 11. Stereographic projection (lower hemisphere) of structural measurements from **a)** the 1045 main ramp crosscut and **b)** the 770 level 11780N crosscut.

is significantly mineralized (25–60 g/t Au) around 8–12 m. It displays strong grunerite development along the chert bands, with local bedding-parallel quartz-carbonate veinlets.

Ore mineralogy and alteration facies of the garnet-grunerite unit (4EA)

Gold ore is mainly constituted of smoky grey to black quartz veins and/or quartz flooding with pyrrhotite and iron-carbonate minerals (Fig. 12a, 13). Pyrrhotite is the dominant sulphide associated with gold mineralization, as chalcopyrite is very rarely seen in hand samples, and traces of arsenopyrite are locally present, but not consistently correlated with gold. In garnet-grunerite layers, pyrrhotite occurs as very fine-grained aggregates along foliation planes and in pressure shadows and filling fractures of coarse, dark red almandine porphyroblasts. Alternating boudinaged chert bands, quartz veins, or quartz-flooded layers contain dark green, fine-grained amphibole, biotite, and locally clinopyroxene, likely hedenbergite. Two end-members of ore can be distinguished: quartz flooding with over 50% quartz and pyrrhotite replacement (up to 40% pyrrhotite). In contrast to the mineralogy proximal to ore zones that includes coarse red euhedral almandine garnet crystals in a green amphibole-biotite matrix, the distal, least-altered 4EA facies rather comprises anhedral to subhedral almandine garnet in a fine-grained grunerite-rich matrix (Fig. 13a).

DISCUSSION

Structural setting and controls on mineralization

Important information on the geometry and structural controls of the Musselwhite deposit was obtained by studying key underground and neighbouring surface exposures

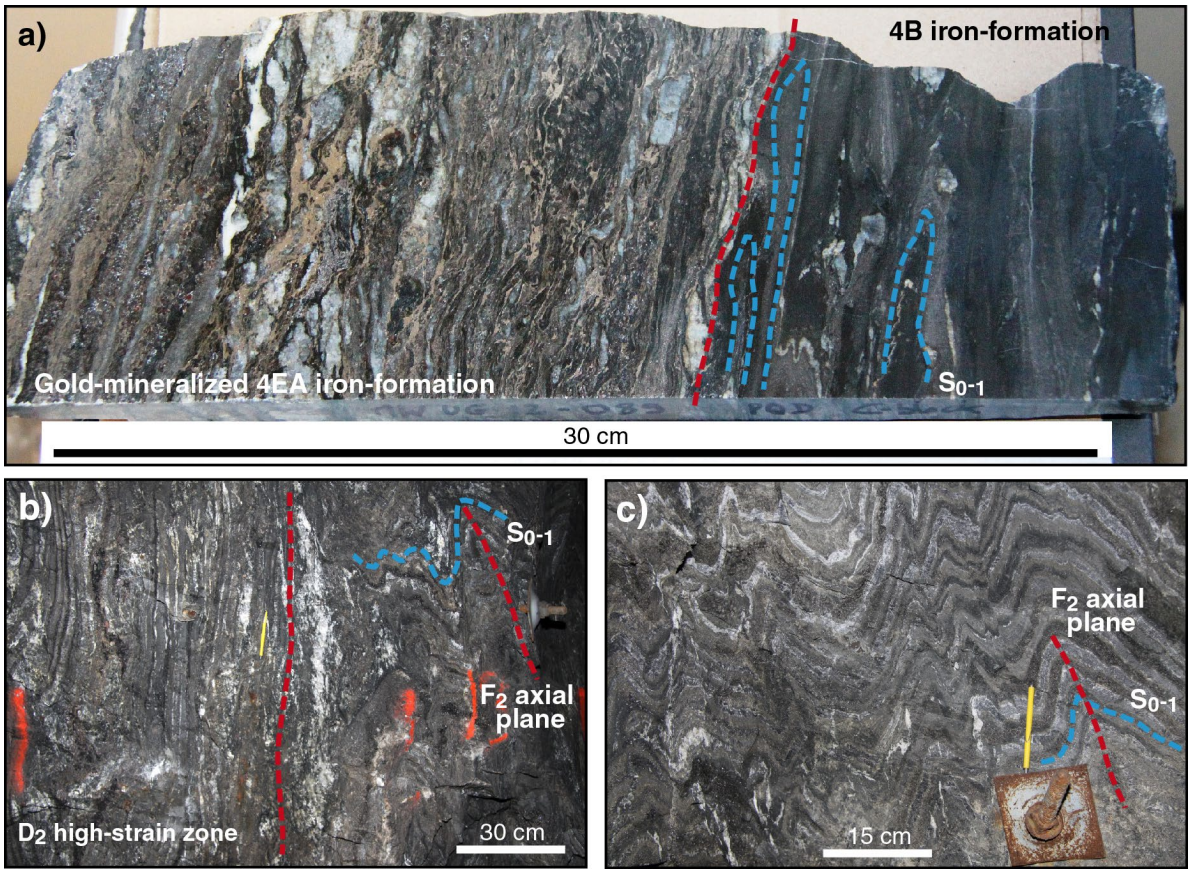

Figure 12. a) Photograph of a polished slab of ore sampled on the north-facing wall of the 770 level 11780N crosscut. Note the contrast in mineralization between the garnet-grunerite unit to the left, which displays intense pyrrhotite replacement and the chert-magnetite unit to the right that is essentially barren. Photograph by W. Oswald; 2014-207. **b)** Photograph of part of the 770 level 11780 crosscut showing the difference in style of deformation and transposition gradient associated with a D_2 high-strain zone involving clastic chert-magnetite iron-formation and garnet-grunerite iron-formation. Photograph by B. Dubé; 2014-202. **c)** Photograph of part of the 770 level 11780N crosscut showing folded chert-magnetite±garnet-amphibole unit cut by subvertical axial-planar veins, bedding-parallel extensional veins, and axial-planar discrete brittle faults. Photograph by B. Dubé; 2014-203

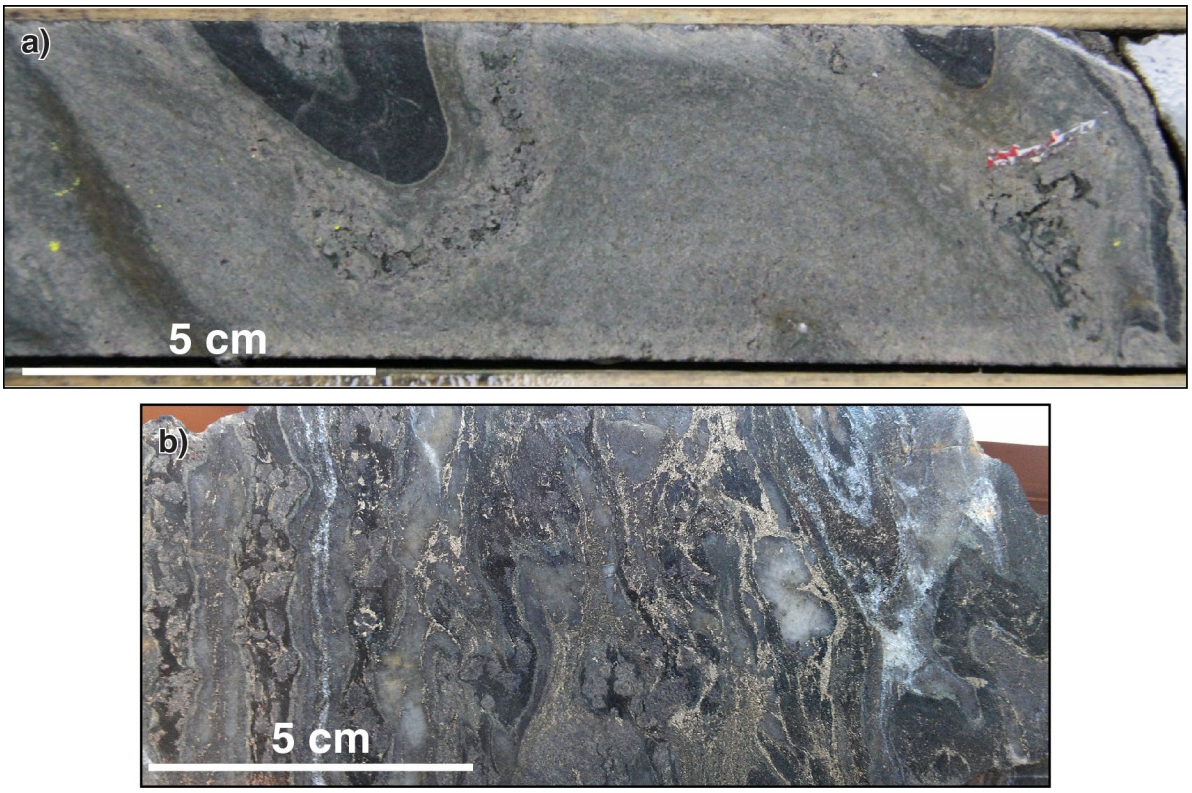

Figure 13. a) Photograph of a drill-core sample of very weakly altered garnet-grunerite iron-formation; 2014-209. **b)** Photograph of a hand sample of gold-bearing, altered, garnet-grunerite iron-formation from the 770 level 11780N crosscut; 2014-206. Both photographs by W. Oswald,

since mesoscopic structures and fabrics are often indicative of megascopic and regional-scale replication of structures and deformation styles.

Surface mapping indicates that although D_2 is the dominant structural phase of the region, older structural fabrics are recognized in zones of lower D_2 strain, such as in the west antiform area. Here, a penetrative S_1 foliation and F_1 folds are affected by F_2 folds and axial-planar S_2 spaced cleavage. F_1 and F_2 folds produce a type 3 interference pattern of Ramsay and Huber (1987), which suggests that F_1 fold axes were nearly coaxial with those of F_2, whereas F_1 axial planes were originally recumbent to shallowly inclined to the southwest. D_2-related structures have a fairly consistent geometry in a specific lithological facies. Small deviations in their orientation can locally occur due to competence contrasts. Other variations, such as opposed plunge directions of F_2 axes may be caused by the interference with earlier F_1 folds or by overprinting F_3 folds. The D_3 deformation phase appears to have fairly restricted impact on the geometry of the stratigraphic package and of mineralized zones. The interference between D_1 and D_2 structures, however, has an important control on the distribution of the prospective banded iron-formation horizons.

In the area south of the Opapimiskan Lake, the presence of two similar volcanic packages comprising high-Mg basalt units and ultramafic flows and sills cored by metasedimentary rocks suggest that a major F_1 fold axis may occur along the trend of Zeemel Lake (Fig. 2a). The geometry of such structure would imply that the stratigraphy of one of the limbs of this isoclinal fold is overturned (Fig. 14). This interpretation is supported by scarce stratigraphic polarity indicators, such as southeast-facing pillowed basalt observed north and west of Zeemel Lake (Fig. 2a), and by recent high-precision U-Pb geochronological data (McNicoll et al., 2013; Oswald et al., 2014) that indicate that the northern limb, including the mine sequence, is inverted and younging downward to the southeast. This new model has implications on the regional distribution of the banded iron-formation horizons, notably those hosting gold mineralization at the Musselwhite mine, and could have considerable impact on regional mineral exploration. More specifically, repetitions of prospective banded iron-formation along refolded limbs of F_1 folds increase the potential areas south of the mine.

The Musselwhite deposit is located in a structural domain of intense deformation in which mineralized zones preferentially occur where D_2 high-strain zones affect specific facies of the northern iron-formation that were chemically prone to react with the gold-bearing fluids (*see* below). D_2 high-strain zones are better developed along the hinge zones and long limbs of tight fold structures, such as the T-antiform or the keel of the PQ deeps synform (Fig. 8). These high-strain zones accommodated folding, transposed the iron-formation

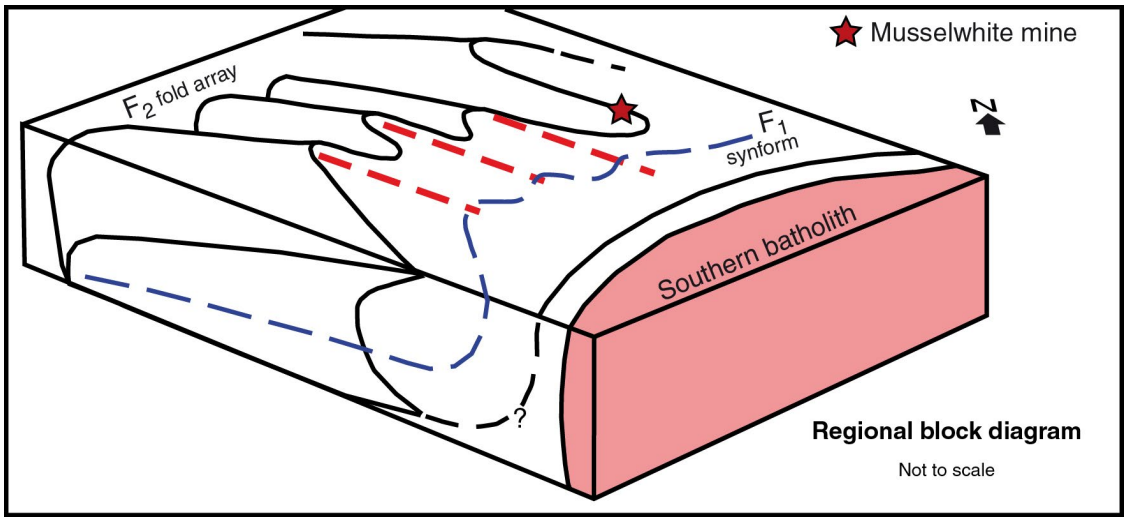

Figure 14. Schematic block diagram of the interpreted regional F_1-F_2 fold interference pattern in the Opapimiskan Lake area.

layers, and apparently acted as pathways toward low-pressure traps for mineralizing fluids (e.g. Cox et al., 2001). In that respect, the bulk of gold mineralization at Musselwhite mine is interpreted as epigenetic and syndeformation (D_2), as originally proposed by Hall and Rigg (1986) for the west anticline mineralized zone.

Lithological controls on mineralization

The garnet-grunerite facies (unit 4EA) hosts most of the gold mineralization. The adjacent clastic chert-magnetite facies (unit 4Bc) can be locally mineralized, whereas the chert-magnetite facies (unit 4B) can be contrastingly barren (Fig. 12), except in rare cases, as in the D-block of the PQ deeps synform area (Fig. 8).

The mapping of the 1045 main ramp crosscut (Fig. 9) provides the basis to better understand the influence of rheological contrasts on the structural and mineralization styles of the various host-rock types. The section also shows the progressive biotite alteration of the overlying mafic rocks, the overprint of carbonate-rich structures, and the minor quartz-pyrrhotite mineralization that locally contains gold. Contrastingly, the 770 level 11780N crosscut is located within the core of an ore zone, where host rocks are strongly deformed and altered, thus providing insights on mineralization processes and proximal footprint. Clear differences in alteration intensity of the garnet-grunerite unit are identified: 1) the high-grade ore in the eastern part of the section displays intense quartz-flooding and pyrrhotite replacement (Fig. 10, 12a, b); 2) the low-grade, strongly altered facies of the western part (Fig. 13b); 3) the barren, moderately altered facies of the 1045 main ramp crosscut; and 4) a distal barren, least-altered dill-core sample (Fig. 13a).

Rheological differences between banded iron-formation facies are part of the controlling factors of mineralization in the garnet-grunerite facies in which gold is widely associated with intense quartz-carbonate veins or quartz flooding. Moreover, as noted by Kolb (2011), the presence of garnet porphyroblasts in the grunerite-rich 4EA facies provides a favourable environment for heterogeneous strain partitioning and favours fluid circulation and gold precipitation in microscopic fractures and pressure shadows. In contrast, the garnet-biotite schist (unit 4F), which also contains garnet porphyroblasts, is much more incompetent and less folded.

Relationships between metamorphism and mineralization

Iron-formation units are extremely reactive to sulphur-bearing fluids and iron and sulphur atoms tend to associate to form pyrrhotite. Pyrrhotite is the most abundant sulphide in the Musselwhite deposit. Such occurrence may originate from the metamorphic conversion of pyrite to pyrrhotite (Tomkins, 2010) or, most likely, because increasing metamorphic conditions favoured the crystallization of pyrrhotite. Given the correlation between pyrrhotite content and gold grade (1% Po ≈ 1 ppm Au; W. McLeod oral comm., 2011) and the high Pearson correlation coefficient between gold and sulphur in preliminary geochemical data (0.5 to 0.8), gold was most probably transported by bisulphide or sulphide complexes ($Au(HS)_2^-$ or $AuHS^0$; e.g. McCuaig and Kerrich (1998)), and released from the solution as sulphur was extracted to crystallize pyrrhotite. Most of the iron is thought to have originated from the breakdown of matrix minerals replaced by grunerite in unaltered lithologies and from amphibole, likely ferrotschermakite to actinolite, in mineralized zones. These replacements are interpreted to reflect CaO enrichment usually associated with orogenic gold mineralization (Dubé and Gosselin, 2007).

Stable isotope data from Musselwhite mine ore (Otto, 2002; Isaac, 2008) has shown that the mineralizing fluids are likely of metamorphic origin, which is compatible with the style and setting of the deposit. Although a magmatic signature is also documented (Isaac, 2008), it is not conclusively linked to gold mineralization nor to the relative chronology of events documented herein. The closest source of metamorphic fluids is the volcanic rocks that structurally underlie the northern iron-formation; however, sediments are also known to be reliable sources of sulphur-bearing and CO_2-rich fluids during metamorphism (Pitcairn et al., 2006; Large et al., 2011). The proposed geological model predicts that the 'lower sediments' adjacent to the mine (Fig. 2b) are also folded underneath the deposit, thus providing an additional potential source for metamorphic fluids that would scavenge metals during syn-D_2 upward flow.

Relative timing of mineralization is best constrained by relationships with the structure and metamorphic paragenesis. The crystallization of grunerite, followed by almandine garnet and the presence of clinopyroxene in iron-formation indicate amphibolite-facies metamorphic conditions (Klein, 2005). Euhedral garnet crystals, such as those observed at the esker docks exposure, overprint the S_2 foliation, indicating they grew late to post-D_2 deformation and suggesting that peak metamorphic temperature occurred during the later stages of D_2 tectonism. In mineralized zones, gold is contained in garnet crystals, including visible gold found along fractures of porphyroblasts or in their pressure shadows, suggesting that mineralization, or its (local) remobilization, occurred after the initiation of porphyroblast crystallization within an active D_2 deformation zone.

CONCLUSION

Detailed surface mapping in the Musselwhite mine area revealed the significance of the early (D_1) deformation that evidently has a strong influence on the geometry and regional distribution of the prospective banded iron-formation horizons. Tight to isoclinal F_1 folds have been refolded, and locally obliterated by D_2 folds and fabrics, which dominate the regional structural pattern. Presence of metre- to decametre-scale F_1 folds coupled with regional geological data and new U-Pb geochronological results on the mine stratigraphy (McNicoll et al., 2013), indicate that the Musselwhite mine occurs along the northern overturned limb of a kilometre-scale F_1 fold, the axis of which lies along Zeemel Lake to the south. Such an interpretation also implies that prospective iron-formation horizons may be present at depth under the mine and repeated to the north and south along limbs of other large-scale F_1 folds, thus providing new regional exploration targets. In the North Caribou greenstone belt of the Opapimiskan Lake area, a strong D_2 strain gradient is documented from North Caribou pluton, increasing northeastward, toward the tectonic contact with the Shade Lake gneissic complex. The Musselwhite deposit is located along a major isoclinal D_2 synform close to this major fault zone. The ore zones are situated at the intersection of steep second-order high-strain zones with the northern iron-formation sequence, as well as along F_2 fold hinges.

Underground mapping emphasizes the importance of structural and stratigraphic control on the distribution of the gold mineralization. The layered anisotropy and rheological contrasts induced by competent banded iron-formation horizons embedded in less competent mafic and ultramafic volcanic rocks strongly influenced deformation styles, both at macro- and microscopic scales, and played an important role in gold-bearing fluid flow, ore formation, and distribution. The rheology and the chemical reactivity to the gold-bearing fluids of the main host banded iron-formation facies (4EA) provided an ideal chemical and structural trap for gold. These observations, as well as the ore mineral assemblage and associated alteration types corroborate that the Musselwhite mine is a syn-D_2 deformation, orogenic gold deposit.

Ongoing work will build on these interpretations to improve knowledge of the complete geological evolution of the deposit with additional detailed surface and underground mapping, lithogeochemical data interpretation, microscopic petrography, and complementary geochronological analyses.

ACKNOWLEDGMENTS

This report emanates from the early results of the Ph.D. thesis undertaken by W. Oswald at the Institut national de la recherche scientifique (INRS-ETE), as part of the Targeted Geoscience Initiative 4 (Lode Gold project) of Natural Resources Canada. Additional support is provided by NSERC, FRQNT, and Goldcorp Canada Ltd., as a BMP scholarship to W. Oswald. The authors sincerely thank Goldcorp Canada Ltd., Musselwhite mine for access to the property, to drill cores and various data sets, and for chartered transport and accommodation. The entire team of the Musselwhite Geology Department is acknowledged for their time, support, interest in this project, and for sharing their unique knowledge of the deposit. The project has also benefited from the collaboration and discussions with D. Schneider, K. Hattori, C. Kelly, E. Gagnon, and O. Bath, all from the University of Ottawa. N. Pinet is acknowledged for his constructive review and astute suggestions.

REFERENCES

Biczok, J., Hollings, P., Klipfel, P., Heaman, L., Maas, R., Hamilton, M., Kamo, S., and Friedman, R., 2012. Geochronology of the North Caribou greenstone belt, Superior Province Canada: implications for tectonic history and gold mineralization at the Musselwhite mine; Precambrian Research, v. 192–195, p. 209–230. doi:10.1016/j.precamres.2011.10.012

Breaks, F.W. and Bartlett, J.R., 1991. Geology of the Eyapamikama Lake area; Ontario Geological Survey, Open File Report 5792, 132 p.

Breaks, F.W., Bartlett, J.R., Osmani, I.A., Finamore, P.F., and Wallace, H., 1985. Opapimiskan Lake project: Precambrian and Quaternary geology of the North Caribou Lake area, district of Kenora, Patricia Portion; *in* Summary of Field Work and Other Activities 1985; Ontario Geological Survey, Miscellaneous Paper 126, p. 268–276.

Breaks, F.W., Bartlett, J.R., de Kemp, E.A., and Osmani, I.A., 1991. Geology of the Doubtful–Akow lakes area, District of Kenora; Ontario Geological Survey, Open File Report 5795, 131 p.

Breaks, F.W., Osmani, I.A., and de Kemp, E.A., 2001. Geology of the North Caribou Lake area, northwestern Ontario; Ontario Geological Survey, Open File Report 6023, 80 p.

Cox, S.F., Knackstedt, M.A., and Braun, J., 2001. Principles of structural control on permeability and fluid flow in hydrothermal systems; Reviews in Economic Geology, v. 14, p. 1–24.

Davis, D.W. and Stott, G.M., 2001. Geochronology of several greenstone belts in the Sachigo Subprovince northwestern Ontario; #18 project unit 89-7; *in* Summary of Field Work and Other Activities 2001; Ontario Geological Survey, Open File Report 6070, p. 18-1 to 18-13.

de Kemp, E.A., 1987. Stratigraphy, provenance and geochronology of Archean supracrustal rocks of western Eyapamikama Lake area, northwestern Ontario; M.Sc. thesis, Carleton University, Ottawa, Ontario, 98 p.

Dubé, B. and Gosselin, P., 2007. Greenstone-hosted quartz-carbonate vein deposits; *in* Mineral Deposits of Canada: a Synthesis of Major Deposit Types, District Metallogeny, the Evolution of Geological Provinces and Exploration Methods (ed.) W.D. Goodfellow; Geological Association of Canada, Mineral Deposits Division, Special Publication No. 5, p. 49–73.

Dubé, B., Mercier-Langevin, P., Castonguay, S., McNicoll, V.J., Pehrsson, S.J., Bleeker, W., Schetselaar, E.M., and Jackson, S., 2011. Targeted Geoscience Initiative 4. Lode gold deposits in ancient deformed and metamorphosed terranes – footprints and exploration implications: a preliminary overview of themes, objectives and targeted areas; *in* Summary of Field Work and Other Activities 2011; Ontario Geological Survey, Open File Report 6270, p. 38–1 to 38–10.

Hall, R.S. and Rigg, D.M., 1986. Geology of the West Anticline Zone, Musselwhite Prospect, Opapimiskan Lake, Ontario, Canada; *in* Proceedings, Gold '86 Symposium; Toronto, Ontario, September 28–October 1, p. 124–136.

Hollings, P. and Kerrich, R., 1999. Trace element systematics of ultramafic and mafic volcanic rocks from the 3 Ga North Caribou greenstone belt, northwestern Superior Province; Precambrian Research, v. 93, p. 257–279. doi:10.1016/S0301-9268(98)00088-6

Isaac, C., 2008. Stable isotope (N, O, H) geochemistry, petrology and compositions of biotite of the Musselwhite mine, Ontario: implications for mineralisation; M.Sc. thesis, Lakehead University, Thunder Bay, Ontario, 133 p.

Kalbfleisch, N., 2013. Crustal-scale shear zones recording 400 m.y. of tectonic activity in the North Caribou greenstone belt, western Superior Province of Canada; M.Sc. thesis, University of Ottawa, Ottawa, Ontario, 162 p.

Klein, C., 2005. Some Precambrian banded iron-formations (BIFs) from around the world: Their age, geologic setting, mineralogy, metamorphism, geochemistry, and origin; The American Mineralogist, v. 90, p. 1473–1499. doi:10.2138/am.2005.1871

Kolb, M., 2011. A microstructural study of Musselwhite mine and Hammond Reef shear-zone-hosted gold deposits; M.Sc. thesis, Lakehead University, Thunder Bay, Ontario, 204 p.

Large, R., Bull, S., and Maslennikov, V., 2011. A carbonaceous sedimentary source-rock model for Carlin-type and orogenic gold deposits; Economic Geology and the Bulletin of the Society of Economic Geologists, v. 106, p. 331–358. doi:10.2113/econgeo.106.3.331

McCuaig, C.T. and Kerrich, R., 1998. P-T-t-deformation-fluid characteristics of lode gold deposits: evidence from alteration systematics; Ore Geology Reviews, v. 12, p. 381–453. doi:10.1016/S0169-1368(98)00010-9

McNicoll, V., Dubé, B., Biczok, J., Castonguay, S., Oswald, W., Mercier-Langevin, P., Skulski, T., and Malo, M., 2013. The Musselwhite gold deposit, North Caribou greenstone belt, Ontario: new high-precision U-Pb ages and their impact on the geological and structural setting of the deposit; Geological Association of Canada–Mineralogical Association of Canada, Abstracts, Winnipeg, Manitoba, May 22–24, 2013, v. 36, p. 142.

Moran, P., 2008. Lithogeochemistry of the sedimentary stratigraphy and metasomatic alteration in the Musselwhite gold deposit, North Caribou Lake belt, Superior Province, Canada: implications for deposition and mineralization; M.Sc. thesis, Lakehead University, Thunder Bay, Ontario, 411 p.

Oswald, W., Dubé, B., Castonguay, S., McNicoll, V., Biczok, J., Mercier-Langevin, P., Malo, M., Skulski, T., 2014. New insights on the structural and geological setting of the world-class Musselwhite gold deposit, Superior Province, northwestern Ontario; Geological Survey of Canada, Open File 7633, 1 poster. doi:10.4095/294817

Otto, A., 2002. Ore forming processes in the BIF-hosted gold deposit Musselwhite mine, Ontario, Canada; M.Sc. thesis, Freiberg University of Mining and Technology, Freiberg, Germany, 86 p.

Piroshco, D. and Shields, H., 1985. Geology and gold mineralization of the Eyapamikama Lake area of the North Caribou Lake greenstone belt, district of Kenora (Patricia portion); *in* Summary of Field Work and Other Activities, 1985, (ed.) J. Wood, O.L. White, R.B. Barlow, and A.C. Colvine; Ontario Geological Survey, Miscellaneous Paper 126, p. 277–286.

Piroshco, D.W., Breaks, F.W., and Osmani, I.A., 1989. The geology of gold prospects in the North Caribou Lake greenstone belt, district of Kenora, northwestern Ontario; Ontario Geological Survey, Open File Report 5698, 94 p.

Pitcairn, I., Damon, A., and Teagle, H., 2006. Sources of metals and fluids in orogenic gold deposits: insights from the Otago and Alpine schists, New Zealand; Economic Geology and the Bulletin of the Society of Economic Geologists, v. 101, p. 1525–1546. doi:10.2113/gsecongeo.101.8.1525

Ramsay, J.G. and Huber, M.I., 1987. The Techniques of Modern Structural Geology – Volume 2: Folds and Fractures; Academic Press, London, United Kingdom, 392 p.

Robert, F., Poulsen, K.H., Cassidy, K.F., and Hodgson, C.J., 2005. Gold metallogeny in the Superior and Yilgarn cratons; *in* Economic Geology, 100th Anniversary Volume, (ed.) J.W. Hedenquist, J.F.H. Thompson, R.J. Goldfarb, and J.P. Richards; Society of Economic Geologists, Inc.; Littleton, Colorado, p. 1001–1033.

Satterly, J., 1941. Geology of the Windigo-North Caribou lakes area, Kenora district (Patricia portion); *in* Ontario Department of Mines, Annual Report for 1939, v. 48, pt. 9, p. 1–32 (accompanied by Maps 48h and 48j, scale 1 inch to 1 mile).

Thurston, P., Osmani, I., and Stone, D., 1991. Northwestern Superior Province: review and terrane analysis; *in* Geology of Ontario, (ed.) P.C. Thurston, H.R. Williams, R.H. Sutcliffe, and G.M. Stott; Ontario Geological Survey, Special Volume 4, pt. 1, p. 80–142.

Tomkins, A., 2010. Windows of metamorphic sulfur liberation in the crust: implications for gold deposit genesis; Geochimica et Cosmochimica Acta, v. 74, p. 3246–3259. doi:10.1016/j.gca.2010.03.003

Van Lankvelt, A., 2013. Protracted magmatism within the North Caribou Terrane, Superior Province: petrology, geochronology, and geochemistry of Meso- to Neoarchean TTG suites; M.Sc. thesis, University of Ottawa, Ottawa, Ontario, 204 p.

Geological Survey of Canada Project 340331NU61